# *The Dynamics of Eukaryotic Replication Initiation: Origin Specificity, Licensing, and Firing at the Single-Molecule Level*

HHS Public Access

Author manuscript

*Mol Cell*. Author manuscript; available in PMC 2016 May 07.

Published in final edited form as:

*Mol Cell*. 2015 May 7; 58(3): 483–494. doi:10.1016/j.molcel.2015.03.017.

# The Dynamics of Eukaryotic Replication Initiation: Origin Specificity, Licensing, and Firing at the Single-molecule Level

**Daniel Duzdevich**[1], **Megan D. Warner**[3], **Simina Ticau**[3], **Nikola A. Ivica**[3], **Stephen P. Bell**[3,4], and **Eric C. Greene**[2,*]

[1]Department of Biological Sciences, Howard Hughes Medical Institute, Columbia University, 650 West 168th Street, New York, NY 10032, United States

[2]Department of Biochemistry and Molecular Biophysics, Howard Hughes Medical Institute, Columbia University, 650 West 168th Street, New York, NY 10032, United States

[3]Department of Biology, Massachusetts Institute of Technology, Cambridge, MA 02139

[4]Howard Hughes Medical Institute, Massachusetts Institute of Technology, Cambridge, MA 02139

## SUMMARY

Eukaryotic replication initiation is highly regulated and dynamic. It begins with the Origin Recognition Complex (ORC) binding DNA sites called origins of replication. ORC, together with Cdc6 and Cdt1, mediate pre-Replicative Complex (pre-RC) assembly by loading a double hexamer of Mcm2-7: the core of the replicative helicase. Here, we use single-molecule imaging to directly visualize *Saccharomyces cerevisiae* pre-RC assembly and replisome firing in real time. We show that ORC can locate and stably bind origins within large tracts of non-origin DNA, and that Cdc6 drives ordered pre-RC assembly. We further show that the dynamics of the ORC-Cdc6 interaction dictate Mcm2-7 loading specificity and that Mcm2-7 double hexamers form preferentially at a native origin sequence. Finally, we demonstrate that single Mcm2-7 hexamers propagate bidirectionally, monotonically, and processively as constituents of active replisomes.

## INTRODUCTION

DNA replication in eukaryotes initiates at many origins of replication throughout the genome. Initiation is regulated to ensure that the genetic material is duplicated only once per cell cycle. Origins in the budding yeast *S. cerevisiae* were first identified as Autonomously Replicating Sequence (*ARS*) elements (Chan and Tye, 1980; Stinchcomb et al., 1980). These



*Correspondence: ecg2108@columbia.edu.

**AUTHOR CONTRIBUTIONS**

D.D. designed, conducted, and analyzed all single-molecule experiments. M.D.W., S.T., and N.A.I. prepared protein samples and M.D.W. and D.D. conducted bulk biochemical assays. D.D. composed the paper with input from all authors, and S.P.B. and E.C.G. directed the project.

are now known to serve as sites of assembly for the pre-RC, which contains at various stages Orc1-6 (ORC), Cdc6, Cdt1, and the Mini Chromosome Maintenance (MCM) proteins Mcm2-7 (Yardimci and Walter, 2014).

ORC was identified through its ATP-dependent ability to bind the native budding yeast origin *ARS1* (Bell and Stillman, 1992). In the context of pre-RC assembly, ORC contributes to the loading of Mcm2-7, the ring-structured core of the replicative helicase (Costa et al., 2014; Evrin et al., 2009; Remus et al., 2009; Sun et al., 2013).

Mcm2-7 loading involves sequential recruitment of two Mcm2-7/Cdt1 heptamers by ORC and Cdc6. The initial loading event is thought to coincide with release of Cdt1 from Mcm2-7/Cdt1 (Fernández-Cid et al., 2013; Sun et al., 2014). A second Mcm2-7/Cdt1 complex is then loaded, yielding a head-to-head double hexamer of Mcm2-7 that encircles dsDNA (Evrin et al., 2009; Remus et al., 2009). Initiation of replication is triggered by Dbf4-Dependent Cdc7 Kinase (DDK) and S-phase Cyclin-Dependent Kinase (S-CDK) (Heller et al., 2011), which stimulate recruitment of Cdc45, GINS, and other factors (Tanaka and Araki, 2013). The resulting Cdc45-Mcm2-7-GINS (CMG) complex eventually functions as the replicative helicase (Costa et al., 2014; Fu et al., 2011; Ilves et al., 2010).

Pre-RC assembly has been studied with bulk *in vitro* assays, yielding many insights into the biochemistry of the pathway, and genetics has been essential to identifying the many factors involved in replication initiation. Single-molecule approaches can further our understanding by addressing the dynamics underlying assembly, origin firing, and subsequent replisome progression.

Here we directly visualize pre-RC assembly and replication initiation in real time at the single-molecule level. Our work reveals that ORC can bind the native *ARS1* origin sequence embedded in 47.5 kbp of nonspecific DNA. Cdc6 mediates an apparent increase in ORC specificity, as previously reported (Speck and Stillman, 2007), and by analyzing the single-molecule binding behavior of ORC and Cdc6 we explain the mechanism underlying this effect. We show how Cdc6 dictates strictly ordered pre-RC assembly, with ORC binding to DNA first, followed by recruitment of Cdc6, and then Mcm2-7/Cdt1. Furthermore, we demonstrate that Cdc6 differentiates *ARS1*-bound ORC from non-*ARS1*-bound ORC thereby contributing to origin selection. We also characterize Mcm2-7/Cdt1 recruitment, and find that Mcm2-7 double hexamers form preferentially at *ARS1* and remain at the origin until replication initiation. Moreover, we show that a single Mcm2-7 double hexamer is necessary and sufficient for origin firing and that a single Mcm2-7 hexamer is sufficient for replisome progression. Our work reveals the variables that direct selective and correct pre-RC formation, and it follows the trajectory of Mcm2-7 from the first to the last steps of replication initiation.

## RESULTS

### A DNA Curtain Assay for Pre-RC Assembly

We used the DNA curtain assay and Total Internal Reflection Fluorescence Microscopy (TIRFM) (Greene et al., 2010) to visualize pre-RC assembly. DNA curtains are prepared by

coating the surface of a sample chamber with a lipid bilayer. The bilayer passivates the surface and functionalized lipids within it provide mobile attachment points for DNA. For single-tethered curtains (Figure 1A, left panel), the bilayer is disrupted at defined locations by nano-patterned chromium barriers, and DNA is aligned along these barriers by the application of buffer flow; because the DNA molecules are only tethered at one end, they disappear from view when buffer flow is paused. Double-tethered curtains (Figure 1A, right panel) use a series of antibody-coated pentagons that anchor the other end of each DNA so that the curtain remains confined in the optical detection volume defined by the penetration depth of the excitation field even in the absence of buffer flow (Gorman et al., 2010).

For these experiments we cloned the native *ARS1* origin into the λ phage genome. The resulting construct, $\lambda_{ARS1}$, contains a single origin of replication embedded within 47.5 kbp of non-origin DNA, with *ARS1* corresponding to just 0.4% of total DNA–mimicking the approximate density of origins in the budding yeast genome (Siow et al., 2012). $\lambda_{ARS1}$ has a skewed AT distribution and contains a total of 26 *ARS* Consensus Sequence (ACS)-like sites, each with at least 9 matches to the 11 bp ACS (Figure 1B).

To assay the DNA-binding activity of ORC using single-tethered DNA curtains, biotinylated ORC was pre-incubated with a four-times molar excess of Quantum Dot (QD) streptavidin conjugate and injected into the sample chamber for two minutes. The labeled ORC construct loads high-salt-wash-stable and replication competent Mcm2-7, although with lower efficiency than the native protein (Figure S1). We applied this test to all constructs in this study as indicated in the Supplemental Figures. Excess protein was then flushed out, and the curtain visualized by TIRFM. These experiments show ORC binding to individual $\lambda_{ARS1}$ molecules (Figure 1C). At a higher concentration, ORC binds to sites distributed along the AT-rich half of $\lambda_{ARS1}$ (Figure 1D and see below). Importantly, ORC disappears from view when buffer flow is paused, confirming that it is bound to the DNA and not adsorbed to the sample chamber surface (Figure 1E).

## DNA Curtains Show the Nature of ORC Specificity

The ORC binding distribution histogram confirms that ORC preferentially associates with the AT-rich half of $\lambda_{ARS1}$, with prominent occupancy near the center of the DNA substrate and the cloned *ARS1* sequence (Figure 2A). ORC binding to *ARS1* was confirmed by comparison to the binding distribution on a λ substrate lacking the *ARS1* site (Figure 2B). ORC's preference for AT-rich sequences agrees with expectations based on the conserved property of eukaryotic ORCs for binding AT-rich DNA (Li and Stillman, 2012) and the high AT content of *ARS* sequences (Siow et al., 2012). Furthermore, unlabeled ORC can load Mcm2-7 at non-*ARS1* sites (albeit with low efficiency), indicating that non-*ARS1*-bound ORC is at least partially biochemically functional (see below). This is predicted by our observation that ORC can bind stably to both ACS-like sequences and *ARS1* with a half life of ~37 minutes (Figure S2): a single long-lived subpopulation of ORC that persists well after excess protein is flushed out. We conclude that the DNA curtain assay can be used to monitor both *ARS1*-specific and nonspecific binding of ORC to individual molecules of DNA.

## ORC Binding Dynamics

To further explore pre-RC assembly dynamics, we looked at the ordered association of each sub-complex. We began by assessing how ORC locates replication origins. For these experiments, ORC was introduced onto a double-tethered DNA curtain and buffer flow quickly terminated, revealing that ORC can locate *ARS1* either by directly binding from solution within our spatial resolution limits (3D search) (Figure 2C) or following a short 1D search along the DNA (Figure 2D).

We can only access information about the fraction of protein-DNA interactions that are stable enough to yield a signal above our temporal resolution (here, 200 ms), so we cannot capture transient collisions between ORC and the DNA. We estimate that at 1 nM ORC, this collision frequency should be ~300 $sec^{-1}$ along each $\lambda_{ARS1}$ molecule (Wang et al., 2013). However, after several minutes of incubation, the number of ORC molecules per DNA is several orders of magnitude lower than if every collision resulted in stable binding (Figure 1D). Therefore, only a subset of these transient collision intermediates is converted to more stably bound states, and this conversion is likelier to occur upon encounter with either *ARS1* or ACS-like sequences.

## Cdc6 can Alter the ORC Binding Distribution

Cdc6 has been reported to increase the selectivity of ORC for origin DNA (Mizushima et al., 2000; Speck et al., 2005; Speck and Stillman, 2007), so we tested directly whether the ORC binding distribution is influenced by Cdc6. In agreement with the prior results, we find that when 1 nM ORC is co-incubated with 4 nM Cdc6, the ORC binding distribution is more *ARS1*-specific (Figure 3A; compare with Figure 2A), with a higher ratio of *ARS1*-bound ORC to non-*ARS1*-bound ORC.

To explore the mechanism underlying this effect, we considered 3 hypotheses. Cdc6 could be (i) increasing the inherent selectivity of ORC for *ARS1* relative to nonspecific DNA, (ii) promoting the dissociation of ORC bound to non-*ARS1* sites, or (iii) transiently sequestering ORC in solution and thereby reducing the effective concentration of free ORC available to bind DNA. This third hypothesis supposes that Cdc6 does not induce a change in ORC binding selectivity, but rather reduces the effective ORC concentration so that highly preferred sites are the more likely to become occupied.

We find, remarkably, that by increasing the ORC and Cdc6 co-incubation time, the specificity effect of Cdc6 is reduced (Figure 3A, inset). This shows that in the presence of excess Cdc6, ORC preferentially populates *ARS1*, but over time also begins to populate less favored non-*ARS1* sites—just as is observed in the absence of Cdc6—suggesting that Cdc6 does not alter the inherent sequence selectivity of ORC.

If the effect of Cdc6 on ORC is a function of the rate at which the DNA becomes occupied by ORC, then the reduced specificity observed at longer incubation times should also be accessible by increasing the ORC and Cdc6 concentrations while keeping the incubation time constant. To test this, we co-incubated 2 nM ORC and 8 nM Cdc6 on a curtain for two minutes and found that indeed the specificity effect is reduced and ORC binds across much of the DNA substrate (Figure 3B). However, if the same concentration of ORC (2 nM) is

incubated on a curtain for two minutes without Cdc6, then the DNA becomes so heavily bound by ORC that it begins to form aggregates across the entire DNA (Figure 3C, top panel). This result strongly suggests that Cdc6 reduces the affinity of ORC for DNA independently of which sites are being bound, and is inconsistent with the hypothesis that Cdc6 alters the binding selectivity of ORC.

We next performed an order-of-addition experiment to determine at which stage Cdc6 exerts its influence on the ORC binding distribution: the addition of Cdc6 after ORC binding does not result in the dissociation of ORC from non-*ARS1* sites (Figure 3C, bottom panel), indicating that Cdc6 exerts its influence before ORC binds DNA.

We next sought to confirm that Cdc6 does not cause ORC to dissociate from non-*ARS1* sites. First, 0.5 nM ORC was bound to the DNA in the absence of Cdc6, free protein flushed out, and a binding distribution measured at two minutes (Figure 3D, cyan). Importantly, the specificity of ORC is distinctly higher under these conditions compared with the 1 nM distribution (see figure 2A), and similar to the Cdc6-induced ORC distribution in Figure 3A ($R^2$ = .91). This demonstrates the relationship between ORC concentration and the specificity of the ORC binding distribution. Then, we measured the distribution after an additional seven minutes and found that it had not changed (Figure 3D, magenta), indicating that ORC dissociates from all stably-bound sites at comparable rates in the absence of Cdc6. Finally 4 nM Cdc6 was injected into the sample chamber and incubated for an additional seven minutes. The final measured distribution had again not changed (Figure 3D, yellow). This result is inconsistent with a model in which Cdc6 promotes the dissociation of nonspecifically bound ORC.

These results argue against models involving either a Cdc6-mediated change in ORC selectivity or Cdc6-mediated ORC dissociation from nonspecific sites, and are most consistent with a model in which the *ARS1*-specificity of the ORC binding distribution is correlated with ORC concentration. Cdc6 forms a stable complex with ORC in solution, but only when ATP hydrolysis is inhibited by ATPγS (Speck et al., 2005). This indicates that ORC and Cdc6 interact in solution, but that this interaction is actively disrupted by ATP hydrolysis. In our hands, under the relatively low ORC concentrations required by single-molecule microscopy, short incubation times, and physiological salt conditions, ORC does not bind DNA in the presence of ATPγS regardless of whether or not Cdc6 is present. This is in contrast to bulk experiments where protein concentrations are typically in the micromolar range. We conclude that the effect of Cdc6 is to reduce the effective concentration of ORC available to bind DNA, probably by forming a transient complex with ORC in solution that cannot bind DNA or has reduced DNA-binding activity. This model makes a specific prediction regarding the order of ORC and Cdc6 recruitment: if the ORC-Cdc6 complex transiently sequesters ORC in solution and prevents it from binding DNA, then pre-RC assembly must occur with ORC binding DNA first, followed by Cdc6 (see below).

### Cdc6 Binding Dynamics

Cdc6 is required for Mcm2-7 loading. We therefore characterized the binding dynamics of fluorescently labeled Cdc6 (Figure S3) to better understand its role in orchestrating pre-RC assembly.

Cdc6 binding to DNA was not detected in the absence of ORC. However, Cdc6 does bind transiently to DNA-ORC (Figure 4A). Binding events are more frequent at *ARS1*-ORC than non-*ARS1*-ORC (Figure 4B), indicating that Cdc6 is likelier to transition into a observably stable bound state if the encountered ORC molecule is at *ARS1*. Under these conditions, ORC occupies sites across the AT-rich half of $\lambda_{ARS1}$ (Figure 3A, inset) so the distribution of the transient Cdc6 binding events is not merely a reflection of the underlying ORC distribution and demonstrates an intrinsic preference for certain DNA-bound ORCs. We estimate that the ratio of the Cdc6 on-rate at *ARS1*-ORC to the Cdc6 on-rate at non-*ARS1*-ORC is ~130, indicating the significant preference of Cdc6 for ORCs at a genuine origin sequence (see Supplemental Experimental Procedures). Furthermore, bound Cdc6 molecules exhibit two distinct lifetimes: $t_{1/2} = 9.6 \pm 0.1$ s for *ARS1*-ORC and $t_{1/2} = 5.5 \pm 0.1$ s for non-*ARS1*-ORC (Figure 4C). These data reveal that Cdc6 can differentiate between ORC bound to *ARS1* and ORC bound to non-*ARS1* sites. This predicts a higher specificity in the Mcm2-7 distribution than the ORC distribution (see below).

### Ordered Recruitment of Pre-RC Components

To test the prediction that Cdc6 directs ordered pre-RC assembly, we performed a two-color experiment in which ORC and excess Cdc6 were co-incubated but differently labeled (Figure 4D). We observe no instances of ORC binding simultaneously with Cdc6 ($n_{\text{ORC binding events}} = 273$), and all Cdc6 binding events occurred with ORC already bound to the DNA ($n_{\text{Cdc6 binding events}} = 24$). This rules out the possibility that Cdc6 directs the selectivity of ORC for specific DNA sites. Furthermore, we observe no instances of ORC-Cdc6 co-dissociation from any site, indicating that Cdc6 does not induce ORC dissociation. Therefore, by ensuring that ORC-Cdc6 co-binding does not happen, Cdc6 dynamics control the order in which pre-RC components assemble: ORC first, then Cdc6, followed by Mcm2-7.

### Mcm2-7 Loading Occurs Preferentially at *ARS1*

The ultimate role of the ORC-Cdc6 interaction is to mediate Mcm2-7 recruitment and loading. For this stage of the pathway we readily observe *ARS1*-specific Mcm2-7 loading in reactions containing 1 nM ORC, 4 nM Cdc6, and 10 nM QD-labeled Mcm2-7/Cdt1 (Figure 5A and Figure S4). Mcm2-7 loading depends strictly on ORC and Cdc6, and is highly dependent on *ARS1*, as anticipated (Figure 5B). Previous reports have found that loaded Mcm2-7 double hexamers can diffuse along DNA when challenged with a high salt wash (Evrin et al., 2009; Remus et al., 2009). We find that a small fraction of Mcm2-7 complexes diffuse along the DNA in the presence of 0.5 M NaCl (1/192), with the vast majority remaining stably bound, without diffusing freely, even when visualized for tens of minutes (Figure S4). We do not know the reason for this apparent discrepancy, however, we can rule out the possibility that our results reflect the behavior of inactive or otherwise

inappropriately loaded Mcm2-7 (see below). It is possible that the large number of molecules in a bulk setting results in a higher sampling of the Mcm2-7 diffusive state.

## Mcm2-7 Loading Requirements

The pathway that leads to Mcm2-7 double hexamer formation involves several multi-subunit components that have to assemble in a specific way and in a specific order to form a functional scaffold for replication initiation. To explore the sequence of these interactions, we performed order-of-addition experiments and determined which subcomponents are required in solution for Mcm2-7 loading (Figure 5C). First, we incubated $\lambda_{ARS1}$ with ORC and Cdc6 together, flushed out unbound proteins, and then introduced free Cdc6 and Mcm2-7/Cdt1. Under these conditions, Mcm2-7 loads on the DNA, confirming that in the presence of Cdc6, the DNA-bound ORC species is sufficient for Mcm2-7 loading. Second, we incubated $\lambda_{ARS1}$ with ORC and Cdc6, flushed out excess proteins, and then introduced Mcm2-7/Cdt1 alone. Under these conditions Mcm2-7 is not recruited to ORC, showing no interaction with DNA-ORC within the temporal resolution of the experiment (200 ms), indicating that free Cdc6 must be present in solution to load Mcm2-7. This result agrees with our finding that Cdc6 is in rapid equilibrium between free and DNA-ORC-bound states, and that removal of free Cdc6 from solution disrupts this equilibrium.

## Mcm2-7/Cdt1 Binds DNA-ORC-Cdc6 Directly

We next observed how Mcm2-7/Cdt1 searches for DNA-ORC-Cdc6. This search mechanism is particularly intriguing because although Mcm2-7/Cdt1 ultimately interacts with DNA, its target site is a DNA-protein complex rather than a specific DNA sequence. This allows for the possibility that major determinants of target identity include contributions from the protein surface of DNA-ORC-Cdc6. Interestingly, real time visualization of MCM2-7/Cdt1 reveals that it searches for DNA-ORC-Cdc6 exclusively by direct binding out of solution (Figure 5D). This is consistent with an Mcm2-7/Cdt1 search for the DNA-ORC-Cdc6 complex rather than just a DNA component of the pre-RC. This result does not preclude the possibility that certain sequences play a role in Mcm2-7 loading after it is recruited by DNA-ORC-Cdc6 (see below).

## Mcm2-7 Double Hexamer Formation Occurs Preferentially at *ARS1*

The precise requirements for Mcm2-7 double hexamer formation are not completely understood. We therefore used the single-molecule Mcm2-7 loading assay to test how the underlying DNA sequence and the presence of free ORC influence double hexamer formation. To assay double hexamer formation we used an Mcm2-7 construct with a dye-tagged MCM4 (Mcm2-7$^{Mcm4\text{-}DY549}$). Mcm2-7$^{Mcm4\text{-}DY549}$ exhibits the same *ARS1*-specific loading as observed for QD-Mcm2-7 (Figure 5E) and enables quantification of the number of Mcm2-7$^{Mcm4\text{-}DY549}$ hexamers loaded at a given site by continuous laser illumination until photobleaching. The majority of Mcm2-7$^{Mcm4\text{-}DY549}$ complexes at *ARS1* exhibit two-step photobleaching (64%), consistent with expectations for double hexamers (Figure 5F). In contrast, most of the Mcm2-7$^{Mcm4\text{-}DY549}$ at non-*ARS1* sites exhibit one-step photobleaching (85%) (Figure 5F). We observe no multiples of two-step photobleaching at any site, and three-step photobleaching at *ARS1* (10%) and two-step photobleaching at non-*ARS1* sites

(15%) may represent false-positive interference from multiple, unrelated sites of single hexamer loading within a single point of resolution. Taken together, these results are consistent with a model in which *ARS1* mediates the loading of one Mcm2-7 double hexamer.

## DNA-bound ORC is Sufficient for Mcm2-7 Double Hexamer Formation

Current models fail to explain how a single ORC can physically load two Mcm2-7 rings (Yardimci and Walter, 2014). One possibility is that the second Mcm2-7 requires one pre-formed ORC-Mcm2-7 complex followed by the recruitment of a second ORC. We therefore performed an order-of-addition experiment to determine whether ORC in solution plays a role in double hexamer formation. ORC was first incubated with the DNA, free protein flushed out, and Mcm2-7$^{Mcm4\text{-}DY549}$/Cdt1 and Cdc6 co-injected without any additional free ORC. Mcm2-7$^{Mcm4\text{-}DY549}$ photobleaching traces at *ARS1* still showed a predominance of two-step events (59%) (Figure 5G). This result demonstrates that free ORC in solution is not required for Mcm2-7 double hexamer formation, ruling out any models that invoke recruitment of additional ORC molecules downstream of initial ORC binding.

## Replication Initiation Requires an Mcm2-7 Double Hexamer

We next sought to directly visualize replication initiation and replisome progression in real time using the DNA curtain assay. First, we tested the $\lambda_{ARS1}$ substrate and pre-RC assembly conditions for replication competence using a previously-established bulk biochemical approach (Gros et al., 2014; Heller et al., 2011; On et al., 2014): $\lambda_{ARS1}$ and Mcm2-7$^{Mcm4\text{-}DY549}$/Cdt1 support robust, DDK- and *ARS1*- dependent replication in the presence of S-phase extract (Figure S5). We translated this approach to DNA curtains by generating Mcm2-7$^{Mcm4\text{-}DY549}$ double hexamers as described above. Loaded Mcm2-7$^{Mcm4\text{-}DY549}$ was then phosphorylated by the addition of DDK and replication initiated by introduction of S-phase extract supplemented with DDK (see below). Under these conditions we observe origin firing as the Mcm2-7$^{Mcm4\text{-}DY549}$ double hexamers separate and two CMG complexes move bidirectionally away from the origin (Figure 6A and 6B) (Yardimci et al., 2010). In the absence of DDK or the presence of 1 μM S-CDK inhibitor Sic1, Mcm2-7$^{Mcm4\text{-}DY549}$ remains stationary, confirming that origin firing is strictly dependent on DDK-mediated phosphorylation of the Mcm2-7 double hexamer and replication-promoting S-CDK activity. In the presence of the DNA polymerase inhibitor aphidicolin we observe no bidirectional firing, although 18% of Mcm2-7$^{Mcm4\text{-}DY549}$ complexes show apparent decoupling while 82% remain stationary (N = 103) (Figure S5). This suggests that the reaction depends on DNA synthesis, as expected for active replication, but that aphidicolin can cause CMG decoupling from the replisome, as previously reported (Walter and Newport, 2000). We conclude that loaded Mcm2-7$^{Mcm4\text{-}DY549}$ double hexamers are functional for replisome formation and replication initiation.

Remarkably, origin firing is highly efficient, with 79% of Mcm2-7$^{Mcm4\text{-}DY549}$ complexes at *ARS1* eventually yielding replication forks (Figure 6C). In contrast, only 13% of Mcm2-7$^{Mcm4\text{-}DY549}$ complexes at non-*ARS1* sites fire (Figure 6C). These proportions are correlated with the proportions of at-least-two-step and one-step photobleaching events at *ARS1* and non-*ARS1* sites (Figure 5F), indicating that loaded Mcm2-7 double hexamers are

highly competent for replication, whereas single Mcm2-7 hexamers, which predominate at non-*ARS1* sites, fail to initiate. In addition, it is possible that factors other than inefficient double hexamer formation at non-*ARS1* sites limit firing efficiency. For all bidirectional firing events, sister replisomes initiate simultaneously within the temporal resolution of this experiment (60–80 s). Furthermore, we only observe one instance of an apparently unidirectional firing event in which one Mcm2-7$^{Mcm4\text{-}DY549}$ hexamer fired while the other remained stationary. Additional rare instances (N = 7) in which only one hexamer was visible at firing likely resulted from the presence of one photobleached or otherwise unlabeled Mcm2-7$^{Mcm4\text{-}DY549}$ hexamer at the origin. Taken together, these observations suggest that replication initiation is highly efficient in our experimental system, and that bidirectional replisomes fire simultaneously.

## Replisome Firing and Fork Progression

We next characterized the properties of actively progressing replisomes using either Mcm2-7$^{Mcm4\text{-}DY549}$ or Cdc45 labeled with fluorescent streptavidin (see below). Interestingly, the lag time prior to origin firing after the introduction of S-phase extract is 54.3 ± 1.4 min. under these experimental conditions (Figure 6D). During this extended lag time, the Mcm2-7 complexes remain stationary and exhibit no detectable evidence of diffusing away from the origin prior to firing. In addition, although this lag is relatively long, origin firing is highly efficient. This suggests that control mechanisms prevent firing until a complete pair of replisomes is assembled at an origin. Furthermore, the loss of each Mcm2-7$^{Mcm4\text{-}DY549}$ signal during replisome progression occurs in a single step, consistent with expectations for either photobleaching or dissociation of one protein complex. This observation suggests that a single Mcm2-7$^{Mcm4\text{-}DY549}$ hexamer is sufficient to support replisome progression.

These experiments also show an average replisome progression rate of 8 ± 0.4 bp/s (Figure 6E), in good agreement with previous *in vitro* and *in vivo* studies (Loveland et al., 2012; Sekedat et al., 2010). Furthermore, replisome progression is monotonic, and we observe no change in progression rate as a replication fork traverses regions of greatly differing AT content (Figure S6). These experiments also enable us to define an apparent replisome processivity, which has a median value of 7.4 kbp (Figure 6F). Note that our estimate of processivity is confounded by photobleaching, replisome collision with the DNA curtain barrier, and the lifetime of the labeling technique for Cdc45 (see below), and is therefore only a lower bound. Future work with more stable fluorophores and longer DNA substrates will be necessary to accurately define replisome processivity.

## DDK is Required During Replisome Assembly

The replisome contains a host of essential components that must be in place before initiation. To begin deconstructing this process we looked at the behavior of Cdc45, which is overexpressed in the S-phase extract with a 3xHA tag (Heller et al., 2011). We pre-labeled Cdc45 with a biotinylated anti-HA $F_{ab}$ fragment coupled to fluorescent streptavidin. With this approach we observed Cdc45 binding to pre-loaded unlabeled Mcm2-7, followed by replisome firing (Figure 6G). We did not observe bidirectional firing with this approach because the Cdc45 labeling technique is inefficient. However, given the results presented

above with Mcm2-7$^{Mcm4\text{-}DY549}$, we assume that replication is bidirectional under these conditions with the second Cdc45 simply not visible due to poor labeling efficiency.

As indicated above for experiments with Mcm2-7$^{Mcm4\text{-}DY549}$, efficient replication initiation requires both DDK phosphorylation of Mcm2-7 prior to the introduction of S-phase extract ($DDK_1$) and supplementation of the S-phase extract with DDK ($DDK_2$). Previous work has indicated that DDK phosphorylates loaded Mcm2-7, an essential step prior to replisome formation (Heller et al., 2011). However, an additional requirement for DDK was unanticipated. To help define the potential role of DDK during later stages of replisome formation we tested whether $DDK_2$ functions before or after Cdc45 binding. These experiments reveal that omission of $DDK_2$ completely abolishes Cdc45 binding to the nascent replisome (Figure 6H). These results confirm that Mcm2-7 phosphorylation is important for efficient replisome activation, but also that the continued presence of DDK is essential to support Cdc45 binding to the nascent replisome.

## DISCUSSION

Our results offer a series of insights into the dynamics of replication initiation and the characteristics of replisome progression (Figure 7).

### DNA-binding Properties of ORC

ORC can bind a single *ARS1* site embedded within a vast excess of nonspecific DNA, although it can also occupy other predominantly AT-rich sites. No other component of the pre-RC exhibits this sequence recognition capacity on its own. Therefore, pre-RC localization is delimited by ORC behavior (Figure 7A). This work shows how each successive pre-RC component builds on the initial DNA-ORC interaction, ultimately leading to functional Mcm2-7 double hexamers.

For any DNA-binding protein, such as ORC, every available DNA sequence is a potential binding site; the probability of binding any given site is non-zero (Berg and von Hippel, 1987). A target such as *ARS1* has a higher probability of being bound by ORC in a defined unit of time. If ORC is incubated with the DNA for longer or at a higher concentration, then the probability of binding all sites increases, and *vice versa*.

For example, it has been reported that ORC specificity is reduced at lower salt concentrations and increased in the presence of competitor DNA (Gros et al., 2014; Rao and Stillman, 1995; Rowley et al., 1995). At lower salt concentrations, a greater number of protein-DNA contacts will be engaged, but at higher salt concentrations these are likelier to be disrupted, thereby favoring the persistence of stable binding to preferred sites. Competitor DNA sequesters ORC, thereby effectively reducing the concentration of ORC available to bind target DNA. Under these conditions nonspecific sites will be very poorly occupied relative to specific sites, resulting in greater apparent protein specificity. Adding competitor DNA does not alter the intrinsic DNA binding specificity of ORC. This interpretation predicts that tuning ORC concentrations will tune specificity, which is precisely what we observe.

### Cdc6 Dynamics and Pre-RC Assembly

Our results show that Cdc6 can alter the ORC binding distribution, and we propose that this occurs through an effective reduction in ORC concentration. This is consistent with the hypothesis that the transient association of ORC and Cdc6 in solution reduces the capacity of the ORC-Cdc6 complex to bind DNA (Figure 7A), the functional consequence of which is ordered pre-RC assembly: DNA bound by ORC, followed by Cdc6, followed by Mcm2-7.

Our work also reveals that Cdc6 does not bind to DNA-ORC persistently, but is in rapid equilibrium between free and DNA-ORC-bound states (Figure 7B). Cdc6 binds preferentially to *ARS1*-ORC and has a longer lifetime on *ARS1*-ORC compared to non-*ARS1*-ORC. The overall result of this behavior is that the DNA-ORC-Cdc6 intermediate exhibits greater *ARS1*-specificty than DNA-ORC alone. This is understandable given that ORC serves other functions in the cell that are not directly related to replication initiation (Palacios DeBeer et al., 2003; Sasaki and Gilbert, 2007; Scholefield et al., 2011); Cdc6 can distinguish between ORC bound to *ARS1* and ORC bound elsewhere without disrupting these other functions. These results support a model in which Mcm2-7 loading specificity is conferred in significant part by differential Cdc6 kinetics (Figure 7C): a specificity mechanism intrinsic to the pre-RC assembly pathway and not dependent on additional *in vivo* conditions (Belsky et al., 2015). This central coordinating role for Cdc6 accords with the cell's tight control over its expression and degradation (Detweiler and Li, 1997; Drury et al., 2000; Piatti et al., 1995).

### Mcm2-7/Cdt1 Recruitment, Double Hexamer Formation, and Origin Licensing

ORC faces an abundance of potential binding sites across the genome whereas Mcm2-7/Cdt1 has only to find DNA-ORC-Cdc6. Our work shows that Mcm2-7/Cdt1 searches for its target exclusively through direct binding out of solution. We also find a predominance of double hexamers at *ARS1* (Figure 7D), revealing that DNA sequence plays some role in double hexamer formation, probably mediated by an *ARS1*-dictated conformation of ORC. Although in budding yeast this results in origin specificity, the same regulatory mechanism could be harnessed in other organisms if the ORC conformational state is dictated by more degenerate origin sequences or other factors. Furthermore, we demonstrate that Mcm2-7 double hexamer formation does not require free ORC in solution, eliminating models involving the recruitment of a second ORC after the first Mcm2-7 hexamer has been loaded (Fernández-Cid et al., 2013; Yardimci and Walter, 2014).

### Replisome Formation and Firing

Previous studies have reported that bulk replication assays with budding yeast S-phase extract are inefficient (Gros et al., 2014; Heller et al., 2011; On et al., 2014). In contrast, we find that replisome firing is highly efficient in the DNA curtain assay; a comparison of the number of Mcm2-7 double hexamers to the number of Mcm2-7 complexes that fire suggests that most or all double hexamers are competent for replication. This difference suggests that some factor(s) necessary for origin firing may be limiting in the extract but do not effect efficiency in the single-molecule assay where the relative concentration of Mcm2-7 double hexamers is much lower than in bulk.

The high efficiency of origin firing in our assay is nonetheless remarkable given the many components that must assemble to form a complete replisome. This high efficiency in the face of a long lag time and the simultaneous firing of sister forks at each origin indicate that replisome formation is precisely coordinated so that all components of both sister replisomes are present prior to origin firing. This suggests that quality control mechanisms sense the status of both replisomes before allowing an origin to fire (Figure 7E). Future work will be necessary to identify the factor(s) that may be involved in this process.

We find that Mcm2-7 double hexamers do not diffuse away from the origin during the long lag prior to firing. This agrees with *in vivo* studies that map the sites of replication initiation to within a narrowly defined region of the *ARS1* sequence (Bielinsky and Gerbi, 1998, 1999; McGuffee et al., 2013). Upon firing, sister replisomes move in opposite directions and each Mcm2-7 hexamer, tracking with its fork, exhibits single-step photobleaching (Figure 7F). We conclude that only one Mcm2-7 double hexamer is necessary for firing and that a single Mcm2-7 hexamer is sufficient for supporting highly processive fork progression. This last conclusion is consistent with data showing that a single CMG accounts for the footprint of a stalled replisome (Fu et al., 2011) and with recent structural work demonstrating that the CMG complex contains only one Mcm2-7 hexamer (Costa et al., 2014).

We observe no abrupt changes in replisome progression as a function of changes in AT content. This implies that the CMG within the context of a complete replisome unwinds DNA actively (Johnson et al., 2007). The monotonic progression of replisomes across differing DNA sequences suggests that strand separation is not rate limiting to replication, consistent with time-resolved ChIP analysis that shows uniform replisome progression throughout the genome (Sekedat et al., 2010). These observations suggest that the eukaryotic replisome has evolved to traverse regions of different sequence composition with similar efficiency.

Finally, our experiments show that DDK activity in the S-phase extract is required for robust association of Cdc45 with the nascent replisome. This requirement may be necessary to maintain the phosphorylation state of Mcm2-7. Alternatively, DDK may be required for the phosphorylation of an unknown protein in the S-phase extract. Further work will be necessary to distinguish between these possibilities.

### Conclusion

This work provides insights into the mechanisms that ensure successful, origin-specific, eukaryotic replication initiation. We anticipate that our approach to single-molecule imaging will continue to yield insights into the molecular mechanisms underlying DNA replication.

## EXPERIMENTAL PROCEDURES

### TIRFM Experiments and Data Analysis

Single-molecule pre-RC experiments were conducted at room temperature in reaction buffer containing 25 mM HEPES (pH 7.6), 12 mM MgOAc, 50 μM ZnOAc, 1 mM DTT, 225 mM KGlut, 3 mM ATP, 20 mM creatine phosphate (Roche), 0.04 mg/ml creatine kinase (Roche), 4 mg/ml BSA (Sigma-Aldrich), 0.03 mg/ml biotin (Sigma-Aldrich) (in all

experiments involving biotinylated protein), and 1 mM Trolox (Sigma-Aldrich) (in all experiments involving organic dyes). Single-molecule replication experiments were performed in a similar buffer, but with 300 mM KGlut and a protochatechuate-based oxygen scavenging system (see Supplemental Experimental Procedures).

Images were acquired at 5 Hz with 200 ms integration time unless otherwise noted. Specifically, Cdc6 lifetime experiments were performed at 12.5 Hz with 80 ms integration time, and replication experiments were performed at 1 frame per 60 or 80 s with 200 ms integration time. Raw TIFF images were analyzed in Fiji (Schindelin et al., 2012) and position distribution histograms and lifetime analyses were generated with custom Python scripts.

Full details describing DNA substrates, protein preparations, biochemical assays, and data analyses are provided in the Supplemental Experimental Procedures.

## Supplementary Material

Refer to Web version on PubMed Central for supplementary material.

## Acknowledgments

We are grateful to members of the Greene and Bell laboratories for helpful conversations. We thank Corentin Moevus for incisive discussions, Colin Kinz-Thomson for insights about kinetic models, Myles Marshall for assistance with the Figure 6 cartoon, and Adam Shoemaker for technical assistance. This work was supported by NIH grants GM082848 (E.C.G.) and GM52339 (S.P.B.), and NSF grant MCB1154511 (E.C.G.). D.D. was supported in part by an award from the Paul and Daisy Soros Fellowships for New Americans and the Columbia University Graduate School of Arts and Sciences. M.D.W. and S.T. were supported in part by an NIH Pre-Doctoral Training Grant (GM007287) and M.D.W. was also supported by an NSF Graduate Research Fellowship (1122374). S.P.B. is an Investigator and E.C.G. an Early Career Scientist with the Howard Hughes Medical Institute.

## References

Bell SP, Stillman B. ATP-dependent recognition of eukaryotic origins of DNA replication by a multiprotein complex. Nature. 1992; 357:128–134. [PubMed: 1579162]

Belsky JA, MacAlpine HK, Lubelsky Y, Hartemink AJ, MacAlpine DM. Genome-wide chromatin footprinting reveals changes in replication origin architecture induced by pre-RC assembly. Genes and Development. 2015; 29:212–224. [PubMed: 25593310]

Berg OG, von Hippel PH. Selection of DNA binding sites by regulatory proteins. Statistical-mechanical theory and application to operators and promoters. Journal of Molecular Biology. 1987; 193:723–743. [PubMed: 3612791]

Bielinsky AK, Gerbi SA. Discrete start sites for DNA synthesis in the yeast ARS1 origin. Science. 1998; 279:95–98. [PubMed: 9417033]

Bielinsky AK, Gerbi SA. Chromosomal ARS1 has a single leading strand start site. Molecular Cell. 1999; 3:477–486. [PubMed: 10230400]

Chan CSM, Tye BK. Autonomously replicating sequences in Saccharomyces cerevisiae. Proceedings of the National Academy of Sciences of the United States of America. 1980; 77:6329–6333. [PubMed: 7005897]

Costa A, Renault L, Swuec P, Petojevic T, Pesavento JJ, Ilves I, MacLellan-Gibson K, Fleck RA, Botchan MR, Berger JM. DNA binding polarity, dimerization, and ATPase ring remodeling in the CMG helicase of the eukaryotic replisome. eLife. 2014; 3:e03273. [PubMed: 25117490]

Detweiler CS, Li JJ. Cdc6p establishes and maintains a state of replication competence during G1 phase. Journal of Cell Science. 1997; 110:753–763. [PubMed: 9099949]

Drury LS, Perkins G, Diffley JFX. The cyclin-dependent kinase Cdc28p regulates distinct modes of Cdc6p proteolysis during the budding yeast cell cycle. Current Biology. 2000; 10:231–240. [PubMed: 10712901]

Evrin C, Clarke P, Zech J, Lurz R, Sun J, Uhle S, Li H, Stillman B, Speck C. A double-hexameric MCM2-7 complex is loaded onto origin DNA during licensing of eukaryotic DNA replication. Proceedings of the National Academy of Sciences of the United States of America. 2009; 106:20240–20245. [PubMed: 19910535]

Fernández-Cid A, Riera A, Tognetti S, Herrera MC, Samel S, Evrin C, Winkler C, Gardenal E, Uhle S, Speck C. An ORC/Cdc6/MCM2-7 Complex Is Formed in a Multistep Reaction to Serve as a Platform for MCM Double-Hexamer Assembly. Molecular Cell. 2013; 50:577–588. [PubMed: 23603117]

Fu YV, Yardimci H, Long DT, Ho V, Guainazzi A, Bermudez VP, Hurwitz J, Van Oijen A, Schärer OD, Walter JC. Selective bypass of a lagging strand roadblock by the eukaryotic replicative DNA helicase. Cell. 2011; 146:931–941. [PubMed: 21925316]

Gorman J, Fazio T, Wang F, Wind S, Greene EC. Nanofabricated racks of aligned and anchored DNA substrates for single-molecule imaging. Langmuir. 2010; 26:1372–1379. [PubMed: 19736980]

Greene EC, Wind S, Fazio T, Gorman J, Visnapuu ML. DNA curtains for high-throughput single-molecule optical imaging. Methods in enzymology. 2010; 472:293–315. [PubMed: 20580969]

Gros J, Devbhandari S, Remus D. Origin plasticity during budding yeast DNA replication in vitro. EMBO Journal. 2014; 33:621–636. [PubMed: 24566988]

Heller RC, Kang S, Lam WM, Chen S, Chan CS, Bell SP. Eukaryotic origin-dependent DNA replication in vitro reveals sequential action of DDK and S-CDK kinases. Cell. 2011; 146:80–91. [PubMed: 21729781]

Ilves I, Petojevic T, Pesavento JJ, Botchan MR. Activation of the MCM2-7 Helicase by Association with Cdc45 and GINS Proteins. Molecular Cell. 2010; 37:247–258. [PubMed: 20122406]

Johnson DS, Bai L, Smith BY, Patel SS, Wang MD. Single-Molecule Studies Reveal Dynamics of DNA Unwinding by the Ring-Shaped T7 Helicase. Cell. 2007; 129:1299–1309. [PubMed: 17604719]

Li H, Stillman B. The origin recognition complex: a biochemical and structural view. Sub-cellular biochemistry. 2012; 62:37–58. [PubMed: 22918579]

Loveland AB, Habuchi S, Walter JC, Van Oijen AM. A general approach to break the concentration barrier in single-molecule imaging. Nature Methods. 2012; 9:987–992. [PubMed: 22961247]

McGuffee SR, Smith DJ, Whitehouse I. Quantitative, Genome-Wide Analysis of Eukaryotic Replication Initiation and Termination. Molecular Cell. 2013; 50:123–135. [PubMed: 23562327]

Mizushima T, Takahashi N, Stillman B. Cdc6p modulates the structure and DNA binding activity of the origin recognition complex in vitro. Genes and Development. 2000; 14:1631–1641. [PubMed: 10887157]

On KF, Beuron F, Frith D, Snijders AP, Morris EP, Diffley JFX. Prereplicative complexes assembled in vitro support origin-dependent and independent DNA replication. EMBO Journal. 2014; 33:605–620. [PubMed: 24566989]

Palacios DeBeer MA, Müller U, Fox CA. Differential DNA affinity specifies roles for the origin recognition complex in budding yeast heterochromatin. Genes and Development. 2003; 17:1817–1822. [PubMed: 12897051]

Piatti S, Lengauer C, Nasmyth K. Cdc6 is an unstable protein whose de novo synthesis in G1 is important for the onset of S phase and for preventing a ‘reductional’ anaphase in the budding yeast Saccharomyces cerevisiae. EMBO Journal. 1995; 14:3788–3799. [PubMed: 7641697]

Rao H, Stillman B. The origin recognition complex interacts with a bipartite DNA binding site within yeast replicators. Proceedings of the National Academy of Sciences of the United States of America. 1995; 92:2224–2228. [PubMed: 7892251]

Remus D, Beuron F, Tolun G, Griffith JD, Morris EP, Diffley JFX. Concerted Loading of Mcm2-7 Double Hexamers around DNA during DNA Replication Origin Licensing. Cell. 2009; 139:719–730. [PubMed: 19896182]

Rowley A, Cocker JH, Harwood J, Diffley JFX. Initiation complex assembly at budding yeast replication origins begins with the recognition of a bipartite sequence by limiting amounts of the initiator, ORC. EMBO Journal. 1995; 14:2631–2641. [PubMed: 7781615]

Sasaki T, Gilbert DM. The many faces of the origin recognition complex. Current Opinion in Cell Biology. 2007; 19:337–343. [PubMed: 17466500]

Schindelin J, Arganda-Carreras I, Frise E, Kaynig V, Longair M, Pietzsch T, Preibisch S, Rueden C, Saalfeld S, Schmid B, et al. Fiji: An open-source platform for biological-image analysis. Nature Methods. 2012; 9:676–682. [PubMed: 22743772]

Scholefield G, Veening JW, Murray H. DnaA and ORC: More than DNA replication initiators. Trends in Cell Biology. 2011; 21:188–194. [PubMed: 21123069]

Sekedat MD, Fenyö D, Rogers RS, Tackett AJ, Aitchison JD, Chait BT. GINS motion reveals replication fork progression is remarkably uniform throughout the yeast genome. Molecular Systems Biology. 2010:6.

Siow CC, Nieduszynska SR, Müller CA, Nieduszynski CA. OriDB, the DNA replication origin database updated and extended. Nucleic Acids Research. 2012; 40:D682–D686. [PubMed: 22121216]

Speck C, Chen Z, Li H, Stillman B. ATPase-dependent cooperative binding of ORC and Cdc6 to origin DNA. Nature Structural and Molecular Biology. 2005; 12:965–971.

Speck C, Stillman B. Cdc6 ATPase activity regulates ORC·Cdc6 stability and the selection of specific DNA sequences as origins of DNA replication. Journal of Biological Chemistry. 2007; 282:11705–11714. [PubMed: 17314092]

Stinchcomb DT, Thomas M, Kelly J, Selker E, Davis RW. Eukaryotic DNA segments capable of autonomous replication in yeast. Proceedings of the National Academy of Sciences of the United States of America. 1980; 77:4559–4563. [PubMed: 6449009]

Sun J, Evrin C, Samel SA, Fernández-Cid A, Riera A, Kawakami H, Stillman B, Speck C, Li H. Cryo-EM structure of a helicase loading intermediate containing ORC-Cdc6-Cdt1-MCM2-7 bound to DNA. Nature Structural and Molecular Biology. 2013; 20:944–951.

Sun J, Fernandez-Cid A, Riera A, Tognetti S, Yuan Z, Stillman B, Speck C, Li H. Structural and mechanistic insights into Mcm2-7 double-hexamer assembly and function. Genes and Development. 2014; 28:2291–2303. [PubMed: 25319829]

Tanaka S, Araki H. Helicase activation and establishment of replication forks at chromosomal origins of replication. Cold Spring Harbor Perspectives in Biology. 2013:5.

Walter J, Newport J. Initiation of eukaryotic DNA replication: Origin unwinding and sequential chromatin association of Cdc45, RPA, and DNA polymerase α. Molecular Cell. 2000; 5:617–627. [PubMed: 10882098]

Wang F, Redding S, Finkelstein IJ, Gorman J, Reichman DR, Greene EC. The promoter-search mechanism of Escherichia coli RNA polymerase is dominated by three-dimensional diffusion. Nature Structural and Molecular Biology. 2013; 20:174–181.

Yardimci H, Loveland AB, Habuchi S, Van Oijen AM, Walter JC. Uncoupling of Sister Replisomes during Eukaryotic DNA Replication. Molecular Cell. 2010; 40:834–840. [PubMed: 21145490]

Yardimci H, Walter JC. Prereplication-complex formation: A molecular double take? Nature Structural and Molecular Biology. 2014; 21:20–25.

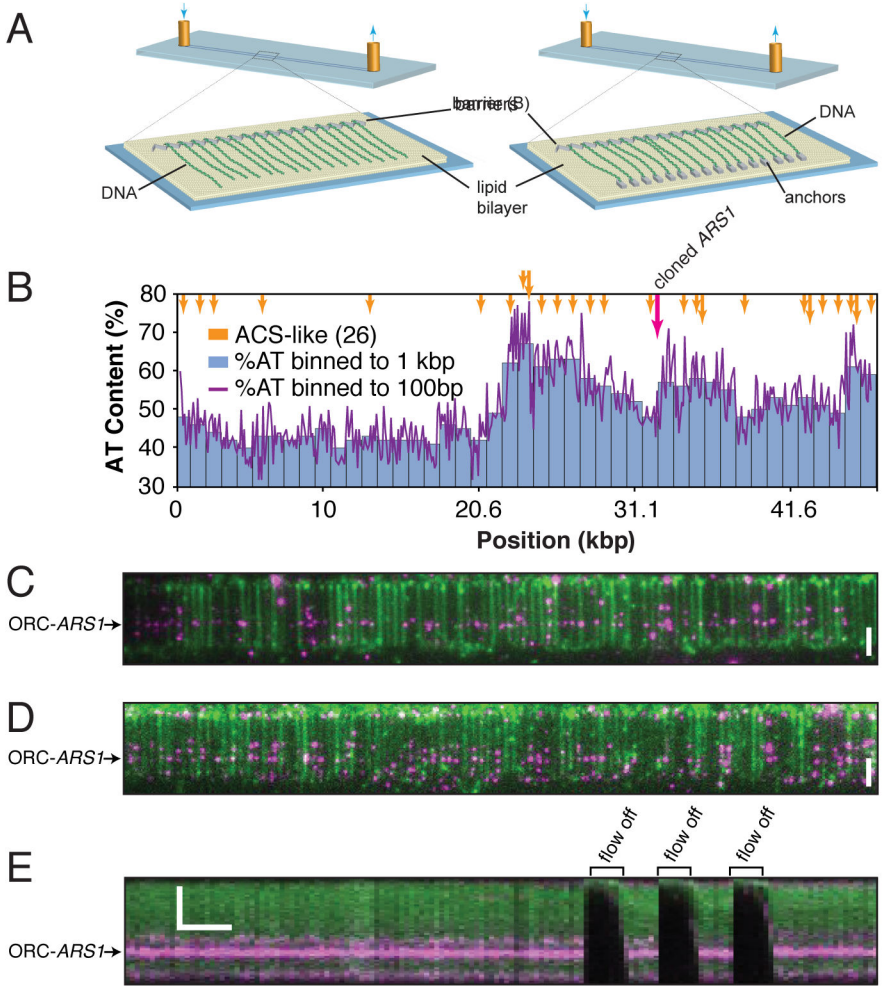


**Figure 1. DNA Curtain Assay for Visualizing pre-RC Assembly**

(A) Schematic of the DNA curtain setup. The left panel shows single-tethered DNA and the right panel shows a double-tethered variation.

(B) AT content and ACS-like sequences of the $\lambda_{ARS1}$ DNA substrate. The magenta arrow indicates the cloned *ARS1* sequence.

(C–D) (C) Wide-field image of a DNA curtain following incubation with 0.5 nM ORC and (D) 1.0 nM ORC.

(E) Kymogram of a single-tethered DNA molecule with bound ORC, showing flow on/off events. See also Figure S1.

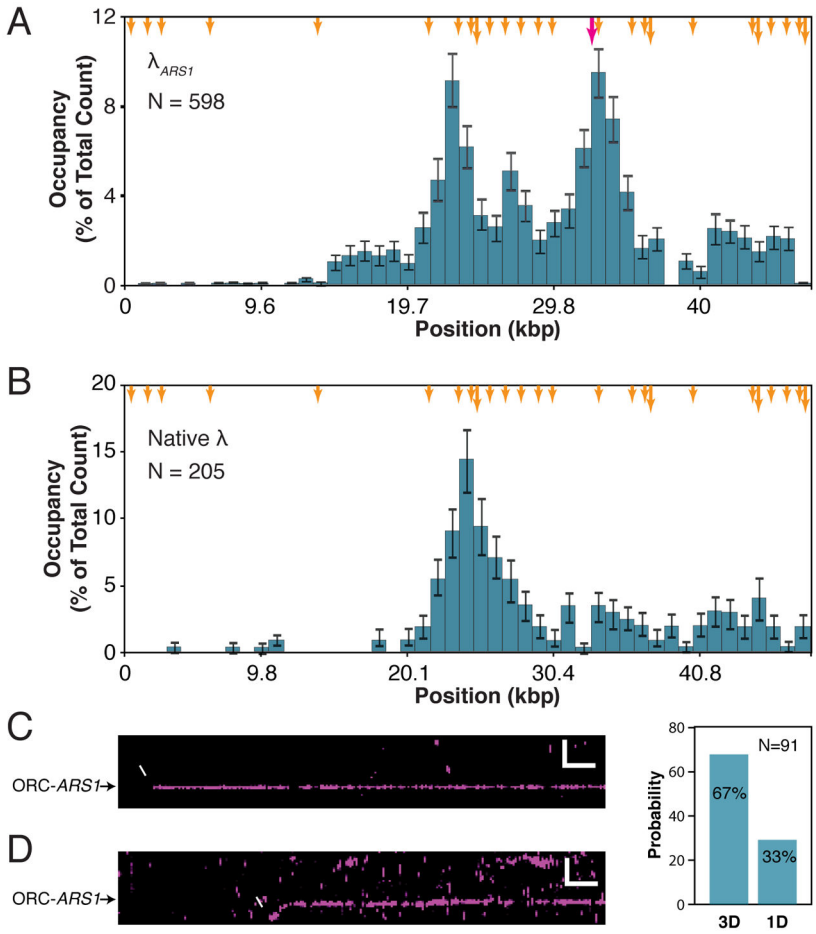


**Figure 2. ORC Binding Distributions**

(A) 1 nM ORC binding distribution histogram on $\lambda_{ARS1}$. Binding positions were scored at a single time point following a 2 minute incubation and the removal of excess protein. For all position distribution histograms, error bars indicate an 85% confidence interval based on 300 bootstrapping samples. N = number of ORC molecules. See also Figure S2.

(B) 1 nM ORC binding distribution histogram on native λ.

(C–D) Kymograms showing examples of (C) ORC binding to *ARS1* directly from solution and (D) 1D sliding of ORC along $\lambda_{ARS1}$ to its target.

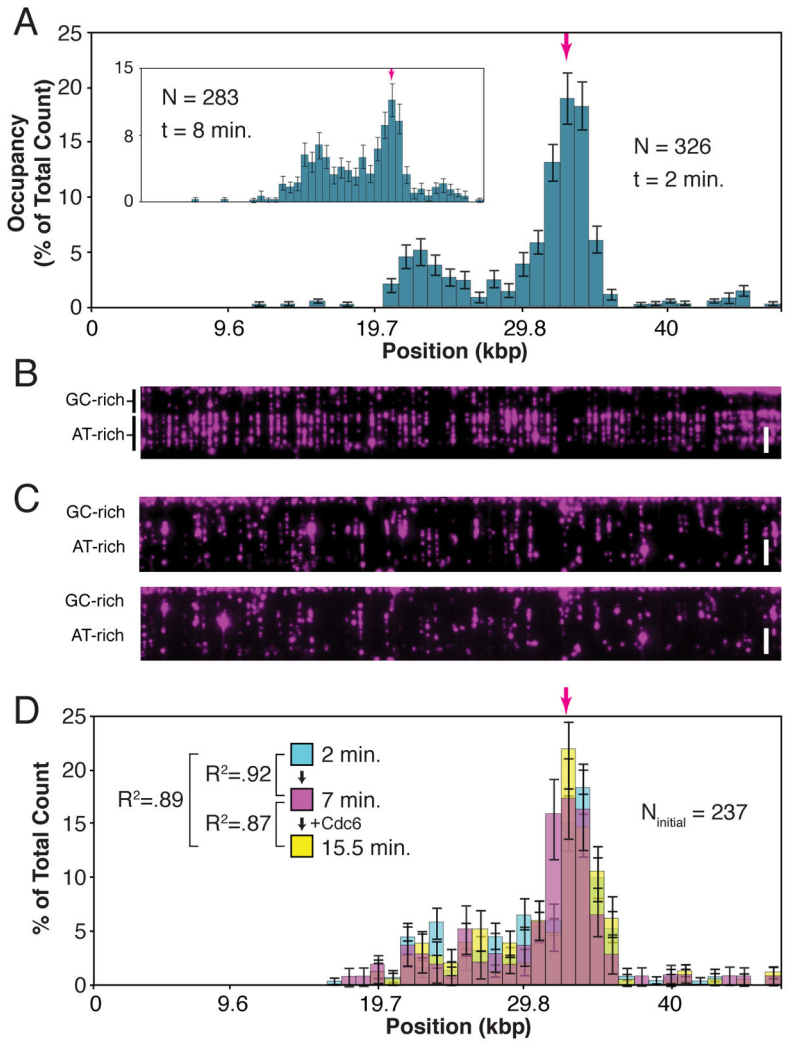


**Figure 3. Cdc6 and the ORC Binding Distribution**

(A) 1 nM ORC binding distribution histogram on $\lambda_{ARS1}$ in the presence of 4 nM Cdc6. The higher specificity is reduced (inset), even in the presence of 40 nM Cdc6, by allowing a longer incubation time of 8 minutes.

(B) 2 nM ORC in the presence of 8 nM unlabeled Cdc6 binds across the AT-rich region of $\lambda_{ARS1}$.

(C) In the absence of Cdc6, 2 nM ORC results in ORC aggregation across the DNA (top panel). Many of the DNA molecules have been ripped from their tethers by the compacting effect of excessive ORC binding. Subsequent addition of 4 nM Cdc6 does not reverse ORC binding (bottom panel).

(D) The initial 0.5 nM ORC distribution (cyan) does not change 7 minutes after excess protein is flushed out (magenta), nor after an additional 7 minutes after Cdc6 is introduced (yellow). (The dead volume of the microfluidics requires 1.5 minutes for the controlled introduction of Cdc6.)

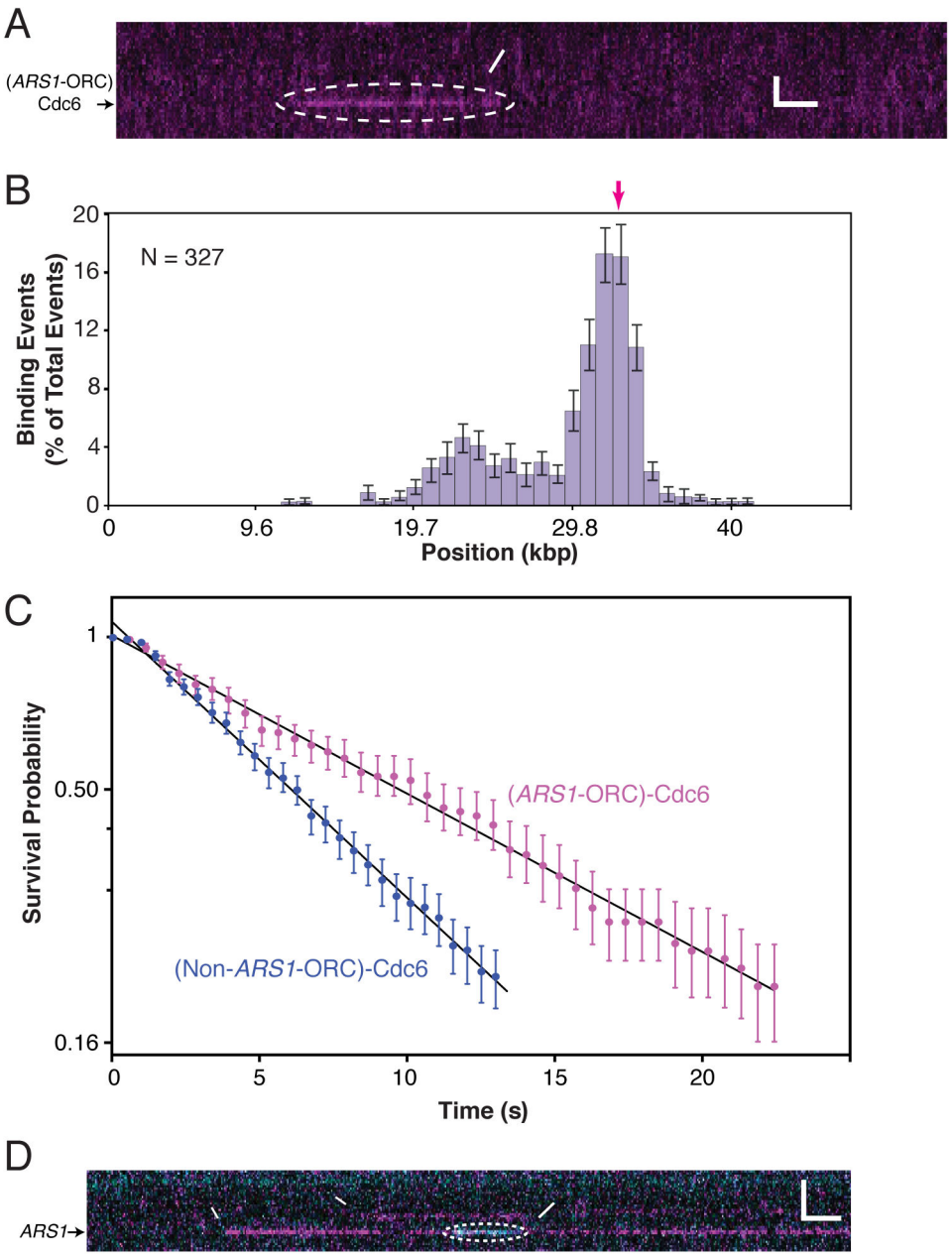


**Figure 4. Cdc6 Binding Dynamics**

(A) Cdc6 labeled with fluorescent streptavidin binds transiently to DNA-ORC (unlabeled). See also Figure S3.

(B) Cdc6 interacts preferentially with *ARS1*-ORC.

(C) The magenta survival probability plot of Cdc6 interacting with *ARS1*-ORC (every 5$^{th}$ 85% CI bootstrapped data point shown, for clarity), and the blue survival probability plot of Cdc6 interacting with non-*ARS1*-ORC (every 6$^{th}$ 85% CI bootstrapped data point shown) are fit with single exponential decay functions. The existence of two lifetimes was ascertained by a statistical F-test ($F = 5024$, $P < .0001$; see Supplemental Experimental Procedures).

(D) Kymogram showing sequential binding of ORC (magenta) and Cdc6 (cyan) to DNA.

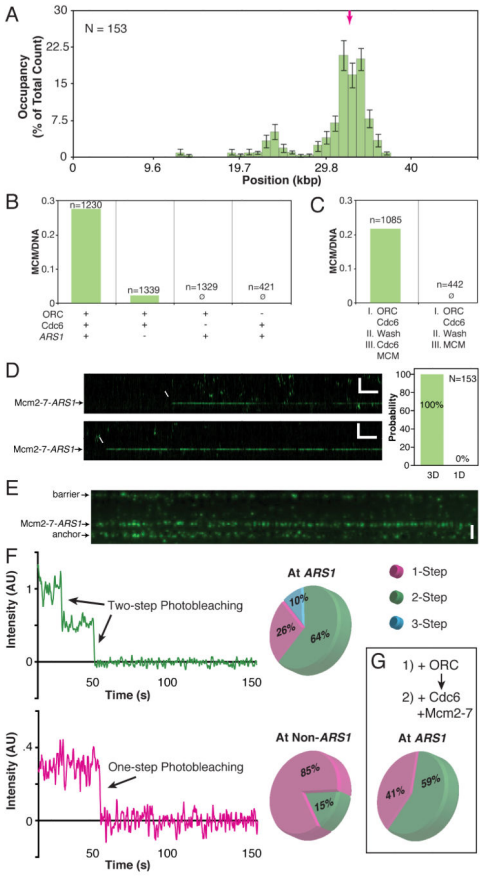


**Figure 5. Cdc6 Dynamics Control Mcm2-7 Specificity**

(A) Mcm2-7 binding distribution histogram on $\lambda_{ARS1}$. See also Figure S4.

(B) Mcm2-7 loading efficiency under various conditions. Mcm2-7 molecules per DNA was quantified by labeling the DNA with the intercalating dye YOYO-1 after the completion of Mcm2-7 loading. N = number of DNA molecules.

(C) Order-of-addition experiment showing that Cdc6 must be present in solution for Mcm2-7 loading.

(D) Kymogram showing direct binding of Mcm2-7/Cdt1 to DNA-ORC-Cdc6. All Mcm2-7/Cdt1 molecules bind DNA-ORC-Cdc6 directly out of solution (right panel).

(E) Wide-field image of Mcm2-7$^{Mcm4\text{-}DY549}$ bound to a double-tethered $\lambda_{ARS1}$ curtain. Proteins nonspecifically associate with the chromium barriers at the top and bottom of the double-tethered curtain, and these regions are excluded from all analyses.

(F) Examples of one-step and two-step photobleaching curves of *ARS1*-localized Mcm2-7$^{Mcm4\text{-}DY549}$. Pie charts show the proportions of 1-step, 2-step, and 3-step photobleaching at *ARS1* (top) and non-*ARS1* sites (bottom).

(G) An order-of-addition experiment shows that ORC is not required in solution to load Mcm2-7 double hexamers.

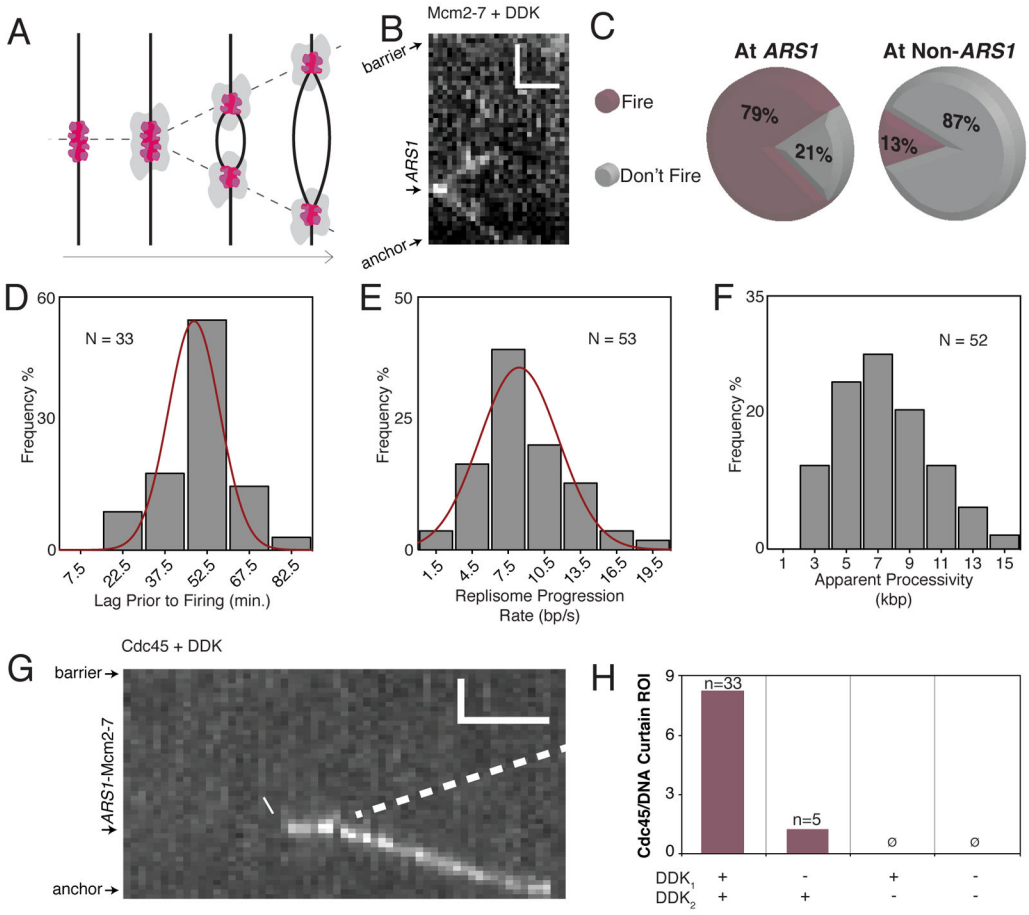


**Figure 6. Replication Initiation and Replisome Progression**

(A) A cartoon of replisome assembly around loaded Mcm2-7 double hexamers and subsequent bidirectional replication. See also Figure S5.

(B) A kymogram of bidirectional Mcm2-7$^{Mcm4\text{-}DY549}$ progression during replication.

(C) Mcm2-7 double hexamer firing is highly efficient.

(D) Replication initiation begins 54.3 ± 1.4 min. after the introduction of S-phase extract (± S.E.M.; σ = 9.9 min.).

(E) The replisome progression rate is 8 ± 0.4 bp/s (± S.E.M.; σ = 3.1 bp/s).

(F) The median apparent processivity is 7.4 kbp.

(G) Cdc45 binds loaded Mcm2-7 and progresses with the replisome. Poor labeling efficiency prevents visualization of the second Cdc45, presumed to progress in the opposite direction (dotted line).

(H) Efficient Cdc45 binding requires prior DDK phosphorylation of Mcm2-7 ($DDK_1$) and supplemented DDK in the S-phase extract ($DDK_2$). The bar graph shows Cdc45 binding efficiency (as number of Cdc45 binding events per Region of Interest, which amounts to four DNA curtains) under different DDK conditions.

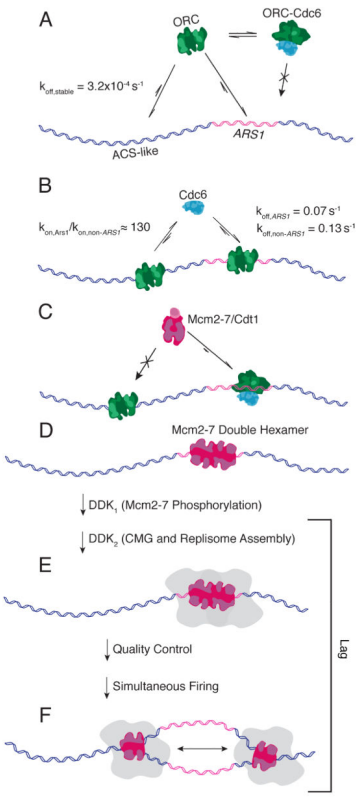


**Figure 7. Schematic of Replication Initiation Dynamics**

(A) ORC has a moderate to high preference for ACS-like sequences and a high preference for *ARS1*.

(B) Cdc6 is likelier to bind *ARS1*-ORC, and once there, bind for longer.

(C) Mcm2-7 interacts only with the DNA-ORC-Cdc6 species.

(D) Mcm2-7 double hexamers form preferentially at *ARS1*. For clarity, the figure depicts only the Mcm2-7 double hexamer. However, our data do not address the presence or absence of other pre-RC components at this stage.

(E) DDK phosphorylation of Mcm2-7 followed by incubation with S-phase extract leads to replisome assembly, but firing of any individual replisome is prevented until both sisters are properly assembled.

(F) Once fully assembled, sister forks fire simultaneously, initiating processive, bidirectional replication.